



A NUMERICAL STUDY OF CONJUGATE GRADIENT DIRECTIONS FOR AN ULTRASOUND INVERSE PROBLEM

XIAODONG ZHANG and SHIRA L. BROCHAT*

*School of Electrical Engineering and Computer Science,
Washington State University, P.O. Box 642752, Pullman, WA 99164-2752, USA*
* *shira@eecs.wsu.edu*

PATRICK J. FLYNN

*Department of Computer Science and Engineering,
384 Fitzpatrick Hall, University of Notre Dame, Notre Dame, IN 46556, USA*
flynn@nd.edu

Received 22 May 2002

Revised 20 March 2004

In ultrasound inverse problems, the integral equation can be nonlinear, ill-posed, and computationally expensive. One approach to solving such problems is the conjugate gradient (CG) method. A key parameter in the CG method is the conjugate gradient direction. In this paper, we investigate the CG directions proposed by Polyak *et al.* (PPR), Hestenes and Stiefel (HS), Fletcher and Reeves (FR), Dai and Yuan (YD), and the two-parameter family generalization proposed by Nazareth (TPF). Each direction is applied to three test cases with different contrasts and phase shifts. Test case 1 has low contrast with a phase shift of 0.2π . Reconstruction of the object is obtained for all directions. The performances of the PPR, HS, YD, and TPF directions are comparable, while the FR direction gives the poorest performance. Test case 2 has medium contrast with a phase shift of 0.75π . Reconstruction is obtained for all but the FR direction. The PPR, HS, YD, and TPF directions have similar mean square error; the YD direction takes the least amount of CPU time. Test case 3 has the highest contrast with a phase shift of 1.003π . Only the YD direction gives reasonably accurate results.

Keywords: Conjugate gradient directions; optimization; inverse problems; imaging.

1. Introduction

Many ultrasound problems of interest involve strong scatterers, and these problems have motivated research on full-wave inversion techniques which make no assumptions about the object. A number of studies have investigated full-wave reconstruction algorithms.^{1–5} However, most of these algorithms are not robust to noise. Over the past several years, a conjugate-gradient (CG) based optimization approach has gained attention because of its insensitivity to noise. A key parameter in the CG method is the conjugate gradient direction which has a significant impact on its performance. The three traditional conjugate gradient directions proposed in the field of nonlinear optimization are the HS (proposed

by Hestenes and Stiefel⁶), FR (proposed by Fletcher and Reeves⁷), and PPR (proposed by Polyak-Polak-Ribiere^{8,9}) CG directions. Recently, a new conjugate gradient direction was proposed by Dai and Yuan¹⁰ (the YD direction), which possesses good convergence properties. Nazareth generalized these four conjugate gradient directions, obtaining a two-parameter family (TPF) of conjugate gradient directions of which the four are members.¹¹ Theoretical and numerical studies of the TPF have yet to be performed.

Since the performance of the CG method depends on the choice of the CG direction, it is worthwhile to investigate which conjugate gradient direction works best for the problem of interest. For electromagnetic inverse imaging, Harada *et al.*¹² have reconstructed strongly scattering objects using the CG method with the PPR direction. Pichot *et al.* have successfully applied the conjugate gradient method to two experimental Ipswich data sets for a metallic circular cylinder and for a metallic strip.¹³ They showed that the CG method with the PPR direction works better than two other choices, namely gradient directions and backpropagation of the error. Kleinman *et al.* proposed a modified gradient method in which the need to solve the direct scattering problem at each step of the iteration is avoided.^{14,15} This significantly reduces the computational requirements. In Ref. 14, they showed that the PPR direction works better than the FR direction. Thus far, researchers have not examined the HS, YD, and two-parameter family conjugate gradient directions for inverse scattering problems. The purpose of this paper is to investigate and compare the TPF, YD, HS, FR, and PPR directions for an ultrasound inverse problem.

One of the main challenges of the inverse scattering problem is obtaining accurate results for large phase shifts which occur when an object is large or its contrast is high. For phase shifts exceeding π , perturbation solutions to the inverse scattering problem fail as shown in Ref. 16. In this paper, we apply the CG method with different CG directions to three test cases with different phase shifts. The size of the problem for each case is $4\lambda \times 4\lambda$, where λ is the wavelength in the background medium. The frequency is chosen to be 400 kHz, and the initial value for all examples is set to zero. For phase shifts up to 0.75π all but the FR CG direction result in reconstruction of the object. Test case 1 has low contrast with a phase shift of 0.2π . Reconstruction of the object is obtained for all directions. The FR direction gives the largest mean square error and requires the greatest amount of CPU time. The performances of the PPR, HS, YD, and TPF directions are comparable in terms of accuracy and CPU time. Test case 2 has medium contrast with a phase shift of 0.75π . The FR direction fails, but the PPR, HS, YD, and TPF directions work well. The mean square error is similar for all four directions, but the YD direction takes the least CPU time. Test case 3 has the highest contrast with a phase shift of 1.003π . The FR, PPR, HS, and TPF directions do not work well for this case, but reconstruction is reasonably accurate using the YD direction.

In the next section, the conjugate gradient method is reviewed, and the different directions are explained. In Sec. 3 numerical results are presented and discussed. Conclusions are given in Sec. 4.

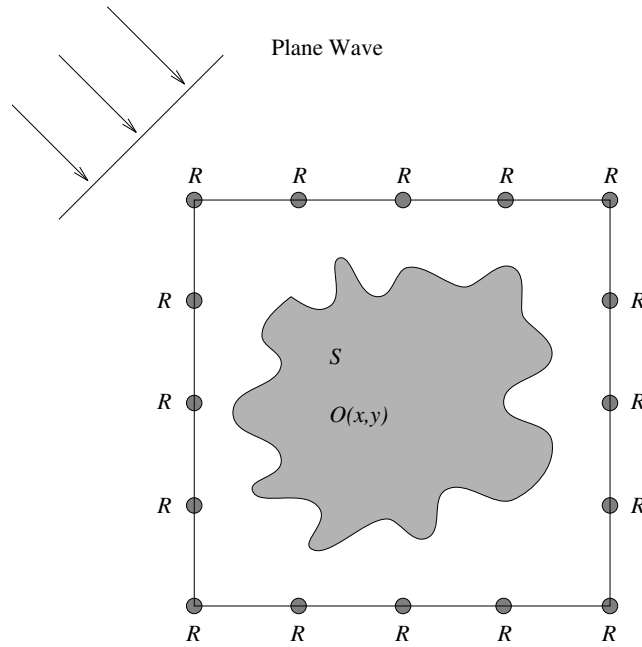


Fig. 1. Scattering geometry.

2. Theory and Formulation

The scattering geometry for the imaging problem is shown in Fig. 1. The object to be reconstructed is labeled S and its physical properties are represented by a vector-valued function $o(\boldsymbol{\rho})$ with $\boldsymbol{\rho} = (x, y)$. Imaging is accomplished by insonifying the object using transducers distributed around it. The scattered ultrasound field is then measured around the object at the receiver locations indicated by R . The acoustic wave equation in two dimensions is expressed in integral form as¹⁷

$$u(\boldsymbol{\rho}) = u_{\text{inc}}(\boldsymbol{\rho}) + \iint_S g(\boldsymbol{\rho} - \boldsymbol{\rho}') o(\boldsymbol{\rho}') u(\boldsymbol{\rho}') d\boldsymbol{\rho}' \quad (2.1)$$

where S is the surface of the object to be imaged in the background medium, $\boldsymbol{\rho} = (x, y)$ and $\boldsymbol{\rho}' = (x', y')$ are the coordinates of the observation point and source point, respectively, $u(\boldsymbol{\rho})$ is the total acoustic pressure field at $\boldsymbol{\rho}$, $u_{\text{inc}}(\boldsymbol{\rho})$ is the incident field at $\boldsymbol{\rho}$, $o(\boldsymbol{\rho})$ is the object function to be reconstructed, and $g(\boldsymbol{\rho} - \boldsymbol{\rho}')$ is the Green's function in two dimensions given by

$$g(\boldsymbol{\rho} - \boldsymbol{\rho}') = \frac{-j}{4} H_0^{(2)}(k_0 |\boldsymbol{\rho} - \boldsymbol{\rho}'|), \quad (2.2)$$

where $H_0^{(2)}$ is the Hankel function of the second kind, $k_0 = \omega/c_0$ is the acoustic wavenumber in the background medium, c_0 is the sound speed of the background medium, and ω is the angular frequency.

Equation (2.1) is linear in u but nonlinear in o . The total field u is the sum of the incident and scattered fields. Thus from Eq. (2.1) we see that the scattered field at a receiver located at $\boldsymbol{\rho}$ is given by

$$u_s(\boldsymbol{\rho}) = \iint_S g(\boldsymbol{\rho} - \boldsymbol{\rho}') o(\boldsymbol{\rho}') u(\boldsymbol{\rho}') d\boldsymbol{\rho}'. \quad (2.3)$$

The object function satisfies the relationship $o(\boldsymbol{\rho}) = k_0^2 [(k^2(\boldsymbol{\rho})/k_0^2) - 1]$, where the term $[(k^2(\boldsymbol{\rho})/k_0^2) - 1]$ is called the contrast of the object function. $k(\boldsymbol{\rho})$ is the wavenumber at $\boldsymbol{\rho}$ and is related to the frequency f , attenuation α , and sound speed c by¹⁸

$$k(\boldsymbol{\rho}) = \frac{2\pi f}{c(\boldsymbol{\rho})} - j\alpha(\boldsymbol{\rho}). \quad (2.4)$$

The goal of inverse imaging is to solve for the object o using knowledge from the scattered field u_s measured at the receivers. When the object function o is given, the total field u can be uniquely determined from Eq. (2.1); this is the forward scattering problem. However, Eq. (2.3) is ill-posed and has no unique solution when both the scattered field u_s and the total field u are given; this is the inverse scattering problem. Direct solution of Eq. (2.3) for o is impossible; instead optimization is used. First, we cast Eqs. (2.1) and (2.3) in matrix form using the method of moments with pulse basis functions and point matching¹⁹ to obtain:

$$\mathbf{u}_{\text{inc}} = \Gamma O \mathbf{u}, \quad (2.5)$$

$$\mathbf{u}_s = K U \mathbf{o}, \quad (2.6)$$

respectively. Γ is an $N \times N$ matrix and K is an $M \times N$ matrix; \mathbf{u}_{inc} is the incident field vector of length N ; \mathbf{u} and \mathbf{o} are the two unknown vectors of length N ; \mathbf{u}_s is a vector of length M ; O and U are $N \times N$ diagonal matrices containing \mathbf{o} and \mathbf{u} , respectively — i.e., $O_{ii} = \mathbf{o}_i$ and $U_{ii} = \mathbf{u}_i$; N is the total number of cells into which the object is discretized; and M is the total number of receivers per view. The elements in Γ and K are given by

$$\Gamma_{ij} = \iint_{S_j} g(\boldsymbol{\rho}(i) - \boldsymbol{\rho}') d\boldsymbol{\rho}'$$

where $\boldsymbol{\rho}$ is defined over the entire domain of the object, and

$$K_{ij} = \iint_{S_j} g(\boldsymbol{\rho}(i) - \boldsymbol{\rho}') d\boldsymbol{\rho}'$$

where $\boldsymbol{\rho}$ is defined only at the receivers. S_j is the area of the j th cell.

In this paper, Eq. (2.5) is solved using the Bi-CGSTAB-FFT method. Conjugate gradient based optimization¹⁵ is used to solve Eq. (2.6). The Bi-CGSTAB method is a variant of the Bi-CG method and has been widely used to solve nonsingular, nonsymmetric linear systems. The computational effort required by the Bi-CGSTAB method is of the same order as required by the Bi-CG method, but its convergence rate is up to twice as fast. It has been shown that for a large number of test cases the Bi-CGSTAB method converges

more smoothly than other Bi-CG variants such as the CG-S method.^{20,21} For Eq. (2.1), the discretization grid is rectangular and, thus, the matrices Γ and K are simply functions of the shifts of the i th and j th cells. This allows the sum in Eq. (2.1) to be efficiently computed via the convolution theorem and the two-dimensional FFT algorithm.

2.1. The conjugate gradient method

The conjugate gradient method^{15,12,20,22} is an iterative technique that can be used to solve optimization problems by making successive approximations to obtain more accurate results at each iteration. It is a nonstationary method which means computations involve information that changes at each iteration. In the CG method, the solution to an optimization problem involves minimization of a cost function. Here the cost function is given by:

$$\begin{aligned}\Phi(\mathbf{o}) &= \frac{1}{2} \cdot w \cdot \sum_{l=1}^L \|\mathbf{u}_s(l) - \mathbf{u}_m(l)\|^2 \\ &= \frac{1}{2} \cdot w \cdot \sum_{l=1}^L \|\mathbf{r}_l\|^2\end{aligned}\quad (2.7)$$

where $\|\cdot\|$ is the Euclidean norm, L is the total number of source positions or views, $\mathbf{u}_s(l)$ is the calculated scattered field, and $\mathbf{u}_m(l)$ is the measured scattered field for illumination by the l th source. The functional Φ is a measure of the discrepancy between the measured and calculated scattered data due to estimation of the object. As proposed in Ref. 15, the weight w is defined by

$$w = \left(\sum_{l=1}^L \|\mathbf{u}_m(l)\|^2 \right)^{-1}$$

where summation is over all the sources. This choice ensures that the amplitude of the incident field has no impact on the functional since \mathbf{u}_s and \mathbf{u}_m are linear in \mathbf{u} , which in turn is linear in \mathbf{u}_{inc} .

The CG method involves several key updating equations:

$$\mathbf{o}_{k+1} = \mathbf{o}_k + t_k \mathbf{d}_k \quad (2.8)$$

$$\mathbf{d}_{k+1} = -\mathbf{g}_{k+1} + \gamma_k \mathbf{d}_k \quad (2.9)$$

where \mathbf{d}_k is the updating direction vector for the object at the k th iteration, γ_k is chosen to ensure that the direction vector is conjugate to all previous directions, and \mathbf{g}_k is the gradient of the cost function at the k th iteration. \mathbf{o}_1 is the initial guess, chosen to be zero for all the examples shown in this paper, and $\mathbf{d}_1 = -\mathbf{g}_1$. Thus, we use the steepest descent direction to start the iteration. The gradient of the cost function is obtained from:

$$\mathbf{g}_k = w \sum_{l=1}^L [\text{diag}(\mathcal{L}(O)\mathbf{u}_{\text{inc}})\mathcal{L}(O)]^* K^\dagger \mathbf{r}_l^k \quad (2.10)$$

where $\mathcal{L}(O) = (I - \Gamma O)^{-1}$, $[\cdot]^*$ indicates the conjugate of $[\cdot]$, K^\dagger is the conjugate transpose of the matrix K defined in Eq. (2.6), \mathbf{r}_l^k is the difference between the measured and calculated scattered data at the k th iteration when the object is illuminated by the l th source, and t_k is the step size taken along the direction \mathbf{d}_k which in this work is found using a one-dimensional inexact line search with Wolfe conditions as termination criteria. For details on Wolfe conditions, see Ref. 23.

In Eq. (2.7), $\Phi(\mathbf{o})$ is to be minimized. This is accomplished iteratively. At each iteration, the vector \mathbf{o} is updated by computing the minimizing direction based on information from the previous iteration. The relative residue error (*RRE*) is then calculated for the new vector \mathbf{o} using

$$RRE = \sqrt{\frac{\sum_{l=1}^L \|\mathbf{u}_s^k(l) - \mathbf{u}_m(l)\|^2}{\sum_{l=1}^L \|\mathbf{u}_m(l)\|^2}} \tag{2.11}$$

where summation is over all the sources, and the superscript k indicates the k th iteration. Iterations are performed until some predetermined value for *RRE* has been reached. This value is chosen empirically.

2.2. Conjugate gradient directions

The conjugate gradient directions of interest are obtained from

$$\begin{aligned} \gamma_k^{\text{FR}} &= \frac{\|\mathbf{g}_{k+1}\|^2}{\|\mathbf{g}_k\|^2} & \gamma_k^{\text{HS}} &= \frac{\langle \mathbf{g}_{k+1}, \mathbf{g}_{k+1} - \mathbf{g}_k \rangle}{\langle \mathbf{d}_k, \mathbf{g}_{k+1} - \mathbf{g}_k \rangle} \\ \gamma_k^{\text{PPR}} &= \frac{\langle \mathbf{g}_{k+1}, \mathbf{g}_{k+1} - \mathbf{g}_k \rangle}{\|\mathbf{g}_k\|^2} & \gamma_k^{\text{YD}} &= \frac{\langle \mathbf{g}_{k+1}, \mathbf{g}_{k+1} \rangle}{\langle \mathbf{d}_k, \mathbf{g}_{k+1} - \mathbf{g}_k \rangle} \end{aligned}$$

where $\langle \cdot \rangle$ denotes the inner product. When the CG method is applied to a quadratic function and an exact line search is used, $\langle \mathbf{g}_{k+1}, \mathbf{g}_{k+1} \rangle = \langle \mathbf{g}_{k+1}, \mathbf{g}_{k+1} - \mathbf{g}_k \rangle$ and $\langle \mathbf{g}_k, \mathbf{g}_k \rangle = \langle \mathbf{d}_k, \mathbf{g}_{k+1} - \mathbf{g}_k \rangle$.²⁴ In this case, the four CG directions reduce to each other, and the solution can be found in at most n steps, where n is the dimension of the problem. However, when the line search is not exact, the four equations are no longer equivalent. In general, when the algorithms are applied to a nonquadratic function and an inexact line search is used, the CG directions differ and lead to different results.²⁵ No particular CG direction is superior to the others for all practical problems — that is, the best direction depends on the application.

The two-parameter family (TPF) for the CG direction is given by¹¹

$$\gamma_k(\lambda, \mu) = \frac{\lambda \langle \mathbf{g}_{k+1}, \mathbf{g}_{k+1} \rangle + (1 - \lambda) \langle \mathbf{g}_{k+1}, \mathbf{g}_{k+1} - \mathbf{g}_k \rangle}{\mu \langle \mathbf{g}_k, \mathbf{g}_k \rangle + (1 - \mu) \langle \mathbf{d}_k, \mathbf{g}_{k+1} - \mathbf{g}_k \rangle} \tag{2.12}$$

where $\lambda \in [0, 1]$ and $\mu \in [0, 1]$ are parameters. It is easy to see that the FR ($\lambda = 1, \mu = 1$), HS ($\lambda = 0, \mu = 0$), PPR ($\lambda = 0, \mu = 1$), and YD ($\lambda = 1, \mu = 0$) directions are just special cases of this family. It is possible that other choices of λ and μ may lead to better results for nonlinear optimization problems. A thorough theoretical and numerical analysis of

Eq. (2.12) is beyond the scope of this paper, but in addition to examining the performance of the four standard directions, several other choices were made for the TPF parameters as described below.

A number of publications explain why the PPR direction usually outperforms the FR direction.^{14,22} For the PPR method, suppose at a particular iteration step $\mathbf{o}_{k+1} \simeq \mathbf{o}_k$, then $\|\mathbf{g}_{k+1}\| \simeq \|\mathbf{g}_k\|$ and from the definition of γ_k^{PPR} we have $\gamma_k^{\text{PPR}} \simeq 0$. Thus, from Eq. (2.9), $\mathbf{d}_{k+1} = -\mathbf{g}_{k+1}$. This means that the new search direction will turn toward the steepest descent direction causing the PPR method to restart itself and recover from this unfavorable situation. However, for the same situation, the FR method would cycle indefinitely and no progress would be made.²² The self-correction of the PPR direction motivated our choice of the first three directions for the TPF given in Table 1. λ was chosen to be $\min(\|\mathbf{g}_{k+1} - \mathbf{g}_k\|, 1)$, ensuring that γ_k is approximately 0 when $\mathbf{g}_{k+1} \simeq \mathbf{g}_k$. The fourth direction in Table 1 was chosen for comparison purposes.

Table 1. Parameter values for four TPF directions.

Choice 1	$\lambda = \min(\ \mathbf{g}_{k+1} - \mathbf{g}_k\ , 1), \mu = \lambda$
Choice 2	$\lambda = \min(\ \mathbf{g}_{k+1} - \mathbf{g}_k\ , 1), \mu = 1.0$
Choice 3	$\lambda = \min(\ \mathbf{g}_{k+1} - \mathbf{g}_k\ , 1), \mu = 0.0$
Choice 4	$\lambda = 0.5, \mu = 0.5$

3. Numerical Results

In this section, we apply the different conjugate gradient directions under consideration to synthetic scattered data for several examples. In these examples, the object to be imaged is defined inside a square domain, as shown in Fig. 1, with dimensions $4\lambda \times 4\lambda$ where λ is the wavelength in the background medium, here water. The domain is discretized into 16×16 cells and successively illuminated by $L = 16$ plane waves equally spaced around the four sides. Measurements are made around the domain at $M = 64$ receivers. The forward scattering problem is solved using the Bi-CGSTAB-FFT method. For some examples, performance of the different directions both with and without noise is examined. By noise, we mean that Gaussian white noise is added to the synthetic scattered data. The signal-to-noise ratio (*SNR*) is defined by

$$SNR = 10 \log_{10} \frac{\|\mathbf{u}_m\|^2}{\|\mathbf{n}\|^2} \quad (3.13)$$

where the Euclidean norm of the exact measured data $\|\mathbf{u}_m\|$ is obtained after a summation over receivers and sources, and \mathbf{u}_m is the scattered field given by Eq. (2.6) with the actual object parameters; \mathbf{n} denotes the random noise and $\|\mathbf{n}\|^2 = 2LM\sigma^2$, where σ^2 is the variance used to generate the Gaussian white noise. L is the total number of sources, and M is the total number of receivers per source.

To quantitatively assess our reconstruction results, we introduce the relative mean square error (MSE) for the reconstructed contrast of the object profile:

$$MSE = \frac{\|\mathbf{o}_n - \mathbf{o}_t\|}{\|\mathbf{o}_t\|} \quad (3.14)$$

where \mathbf{o}_t is the true contrast and \mathbf{o}_n is the estimated object profile at the n th iteration. In practical applications, the MSE is unknown since \mathbf{o}_t is unknown.

For all the examples, the initial guess is chosen to be zero. Simulations are performed on an HP9000 workstation with 256 MB of memory.

3.1. Test case 1

In the first configuration, the object to be reconstructed consists of two cylinders as shown in Fig. 2. The contrast of the outer cylinder is $(-0.111, -3.24 \times 10^{-3})$ and of the inner cylinder $(-0.123, -7.396 \times 10^{-3})$, where the contrast is defined by $[(k^2(\boldsymbol{\rho})/k_0^2) - 1]$. The phase shift is 0.20π . This object has low contrast, and the phase shift is small. The iterations terminate when either the RRE is less than 1.0×10^{-6} or 150 iterations have been performed. When the former is true, we consider the solution to have converged.

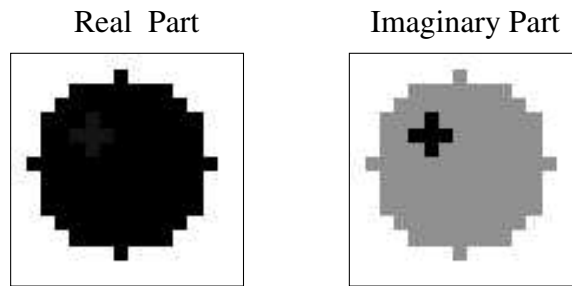


Fig. 2. True contrast for test case 1.

For the noiseless case, all CG directions give acceptable results. The reconstructed images at the 150th iteration are shown in Fig. 3 for the HS direction. The reconstructed (dashed line) and true (solid line) values are compared along a slice through the center of the inner cylinder and agree well. Results using the YD, PPR, and TPF directions (not shown) are similar in image quality to that of the HS direction. However, the reconstructed images using the FR direction are very noisy.

In Table 2, we list the CPU time, RRE values, and MSE values at the 150th iteration for test case 1 without noise for the eight directions considered. The FR direction took the longest time and had the worst RRE and MSE values. The HS direction seems to be the best direction since it took the shortest time and resulted in the smallest RRE and MSE values. The performances of the YD, PPR, and TPF directions are very similar.

To test the performance of the different directions with noise, we added white Gaussian noise to the synthetic scattered data with an $SNR = 50$ dB. All the directions gave

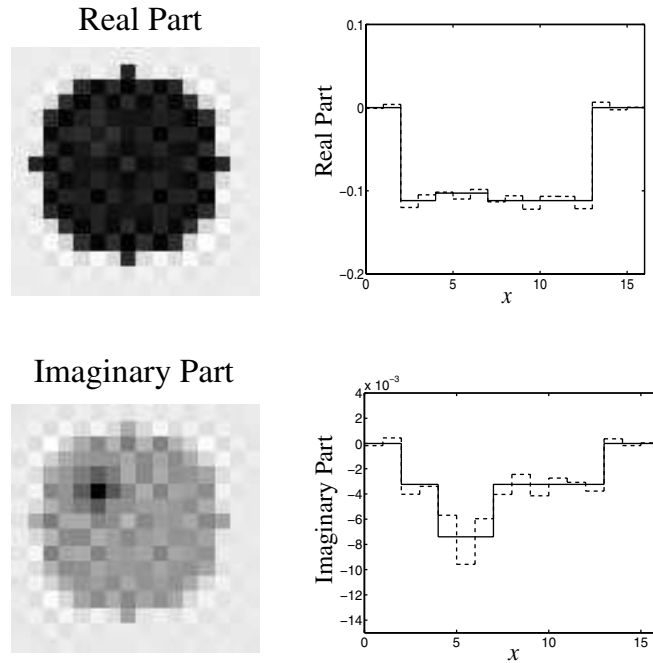


Fig. 3. Reconstructed images using the HS direction for test case 1 without noise. In the right column, the solid line is the true value along a line through the center of the inner cylinder; the dashed line is the reconstructed value along the same line.

Table 2. Comparison of conjugate gradient directions for test case 1 without noise.

	CPU time(s)	$RRE_{150}(10^{-3})$	$MSE_{150}(10^{-2})$
FR	8776.5	124.800	12.4811
HS	1026.3	0.9286	8.1255
PPR	1319.1	1.0421	8.4157
YD	1145.9	3.3822	9.0430
Choice 1	1012.9	1.0339	8.1932
Choice 2	1197.3	0.9621	8.1515
Choice 3	1037.4	1.0342	8.2347
Choice 4	1166.5	1.3255	8.8100

reasonable reconstructions of the object. The reconstructed images using the HS direction are shown in Fig. 4, again with a comparison of the reconstructed and true values along a slice through the middle of the inner cylinder. The results using the FR direction are very noisy, and the quality is almost unacceptable. The reconstructed images from the other directions are quite good and are comparable to each other. The CPU time, RRE values, and MSE values are listed in Table 3. The HS direction seems to work best for this noisy situation.

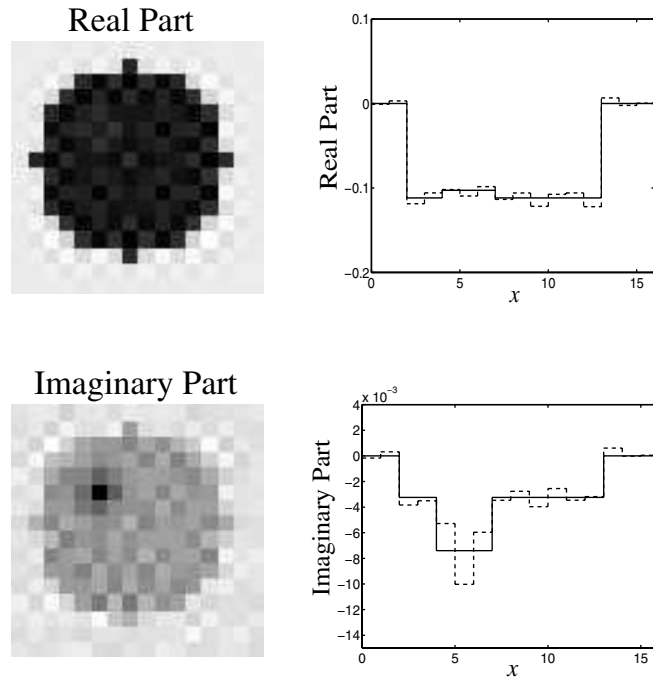


Fig. 4. Reconstructed images using the HS direction for test case 1 with noise, $SNR = 50$ dB. In the right column, the solid line is the true value along a line through the center of the inner cylinder; the dashed line is the reconstructed value along the same line.

Table 3. Comparison of conjugate gradient directions for test case 1 with noise, $SNR = 50$ dB.

	CPU time(s)	$RRE_{150}(10^{-3})$	$MSE_{150}(10^{-2})$
FR	9200.8	124.8134	14.8229
HS	1077.1	2.7527	8.1442
PPR	1860.4	2.8548	8.6997
YD	1146.2	4.2667	9.0497
Choice 1	1016.7	2.7614	8.3121
Choice 2	1375.1	2.7580	8.2348
Choice 3	1061.7	2.7669	8.3910
Choice 4	1170.3	2.9173	8.8219

3.2. Test case 2

For test case 2, the object also consists of two cylinders, one enclosing the other. The contrast for the outer cylinder is $(-0.2103, -0.2126)$ and for the inner cylinder $(-0.435, -0.650)$. The true object is shown in Fig. 5. The phase shift for this object is 0.75π , and the relatively high contrast makes the problem more ill-posed. The termination conditions are the same as for test case 1.

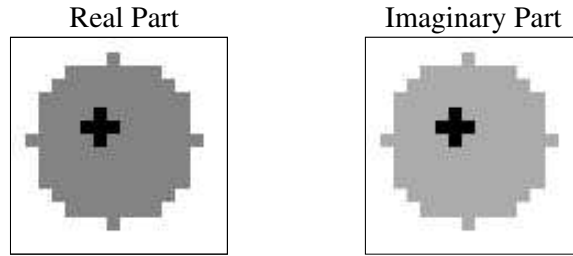


Fig. 5. True contrast for test case 2.

All the directions gave successful reconstructions of the object. The reconstructed images using the YD direction are shown in Fig. 6. The reconstructed and true values are in good agreement. The reconstructed images for the other directions revealed the same high quality as for the YD direction. Not surprisingly, the reconstructed images using the FR direction are very noisy and marginally acceptable. In Table 4, we list the CPU times, *RRE* values, and *MSE* values. From this table, it appears that Choice 3 works slightly better than the HS, PPR, YD, Choice 1, Choice 2 and Choice 4 directions in terms of convergence to the *RRE* and *MSE* values. Interestingly, the YD direction took much less CPU time than the other directions. In fact, for test case 2, the YD direction took only 1.6% more CPU time than it took for test case 1, whereas the other directions took approximately 300% more CPU

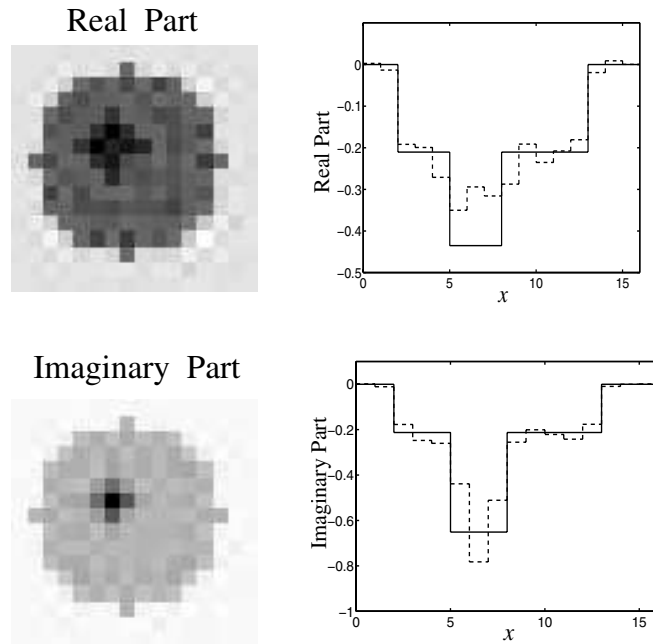


Fig. 6. Reconstructed images using the YD direction for test case 2 without noise. In the right column, the solid line is the true value along a line through the center of the inner cylinder; the dashed line is the reconstructed value along the same line.

Table 4. Comparison of conjugate gradient directions for test case 2 without noise.

	CPU time	$RRE_{150}(10^{-3})$	$MSE_{150}(10^{-1})$
FR	13321.6	95.9911	3.8444
HS	5420.7	3.2487	1.6525
PPR	7193.6	3.2830	1.6425
YD	1163.9	6.2838	1.7752
Choice 1	3839.3	4.2960	1.6697
Choice 2	6262.1	4.2217	1.6748
Choice 3	6505.8	3.0348	1.6263
Choice 4	3659.8	4.0099	1.6578

time. In part, this is because it takes less time to find the step size t_k for every CG iteration with the YD direction than it takes for other directions. For purposes of comparison, the YD results were run until an RRE of 3×10^{-3} was reached. This required a CPU time of 2431.2 s, still appreciably smaller than for the other directions. The numbers in Table 4 are significantly larger than those in Table 2 because test case 2 is more difficult to solve than test case 1.

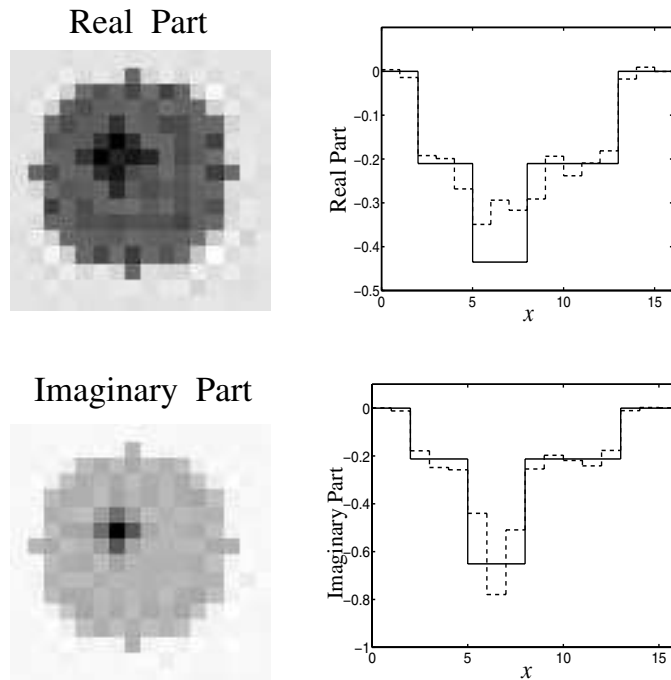


Fig. 7. Reconstructed images using the YD direction for test case 2 with noise, $SNR = 50$ dB. In the right column, the solid line is the true value along a line through the center of the inner cylinder, and the dashed line is the reconstructed value along the same line.

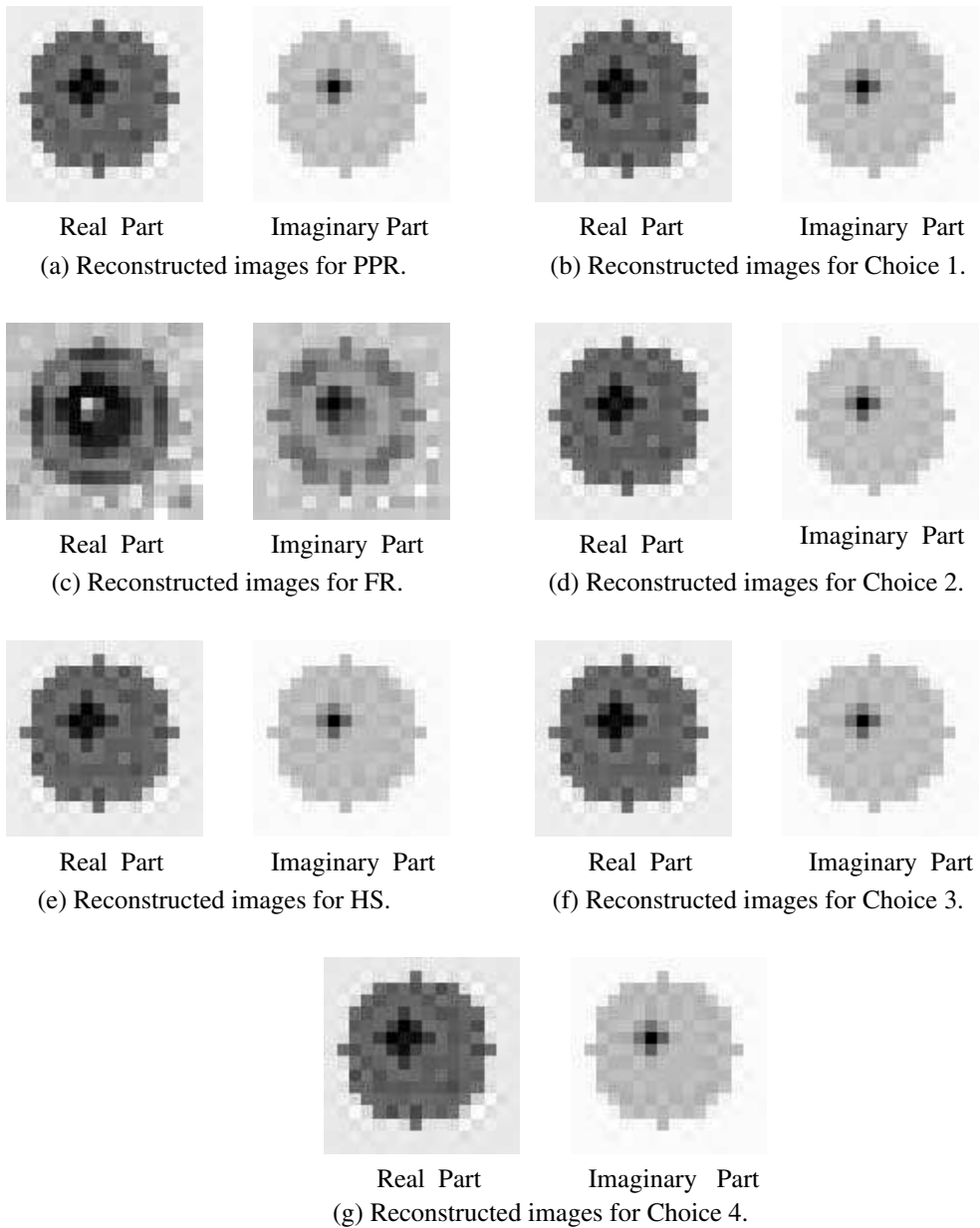


Fig. 8. Reconstructed real and imaginary parts for test case 2 with noise, $SNR = 50$ dB, using the PPR, HS, FR, Choice 1, Choice 2, Choice 3, and Choice 4 directions.

For an SNR of 50 dB, the reconstructed images using the YD direction are shown in Fig. 7 with the reconstructed value along a line through the center of the inner cylinder and the true value along the same line; the reconstructed value matches the true value very well. The other directions also led to successful reconstruction of the object as shown in Fig. 8. In Table 5, we list the CPU times, RRE values, and MSE values. Except for the FR direction,

Table 5. Comparison of conjugate gradient directions for test case 2 with noise, $SNR = 50$ dB.

	CPU time	$RRE_{150}(10^{-3})$	$MSE_{150}(10^{-1})$
FR	13512.2	96.0651	3.8445
HS	6031.6	4.3534	1.6592
PPR	7382.7	4.5543	1.6593
YD	1687.9	6.8283	1.7774
Choice 1	4392.8	4.6607	1.6935
Choice 2	7291.7	4.6268	1.6897
Choice 3	7474.4	4.0835	1.6328
Choice 4	4276.4	4.8221	1.6634

the RRE and MSE values are very close to each other. The RRE and MSE values for the YD direction are slightly larger than those for the HS, PPR, Choice 1, Choice 2, Choice 3, and Choice 4 directions, but the YD direction took much less CPU time than the other directions. There is less difference in the RRE values for the noiseless and noisy results for test case 2 than for test case 1. This is attributed to the greater contrast and phase shift in test case 2.

Notice that when the object is of high contrast, a small RRE does not guarantee a small MSE . This is understandable because the problem is inherently ill-posed. For example, in Table 5, the Choice 2 direction has $RRE = 4.6268 \times 10^{-3}$ and $MSE = 1.6897 \times 10^{-2}$ while Choice 4 has a larger $RRE = 4.8221 \times 10^{-3}$ and smaller $MSE = 1.6634 \times 10^{-2}$. Ideally, the goal of quantitative inverse imaging is to reduce both the MSE and RRE values, but in the real world, the MSE value is unavailable. Regularization terms in the cost functional (for example, as proposed in Ref. 13) can be used to minimize this problem.

3.3. Test case 3

For test case 3, the phase shift of the object is 1.003π . The contrast of the outer cylinder is $(-0.365, -0.191)$ and of the inner $(-0.1656, -0.16973)$. The true object is shown in Fig. 9.

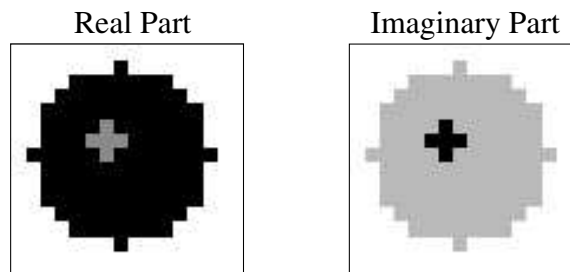


Fig. 9. True contrast for test case 3.

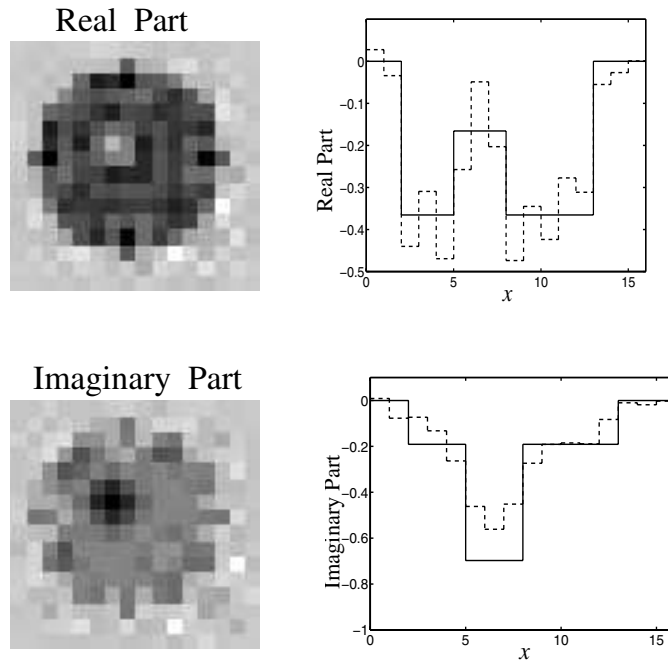


Fig. 10. Reconstructed images for test case 3 without noise using the YD direction.

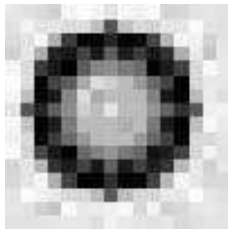
The algorithm terminates when either the RRE is less than 1.0×10^{-6} or 250 iterations are reached.

For the noiseless scattered data, the reconstructed images using the YD direction are shown in Fig. 10. The two cylinders are noticeable in both the imaginary and real parts of the reconstructed images. Comparison of Fig. 6 with Fig. 10 shows the quality of reconstruction for test case 3 has degraded seriously due to the higher phase shift and contrast. The reconstructed images for the other directions are shown in Fig. 11. For these directions, reconstruction of the real image is partially successful, but reconstruction of the imaginary image fails. The high contrast and large phase shift of test case 3 prevents a good quantitative reconstruction of the object even for the noiseless situation.

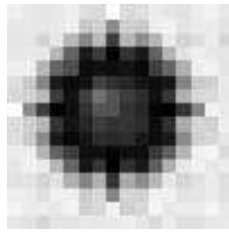
4. Conclusions

It is well-known that the choice of a conjugate gradient direction has a significant impact on the performance of the CG method when applied to a specific problem. In this paper, we considered eight conjugate gradient directions, all variations of the two-parameter family, for an ultrasound inverse problem. The numerical performance for three test cases with small to large phase shifts was investigated. Initial guesses for all the examples were set to zero.

It was found that the FR direction works poorly for all the examples in terms of the quality of the reconstructed images. For a phase shift of about 0.2π , the other directions

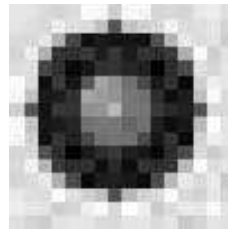


Real Part

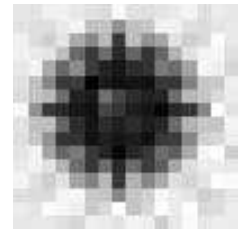


Imaginary Part

(a) Reconstructed images for PPR.

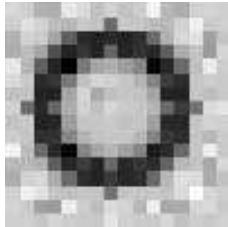


Real Part

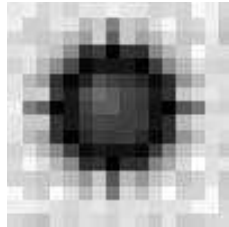


Imaginary Part

(b) Reconstructed images for Choice 1.

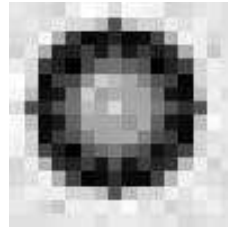


Real Part

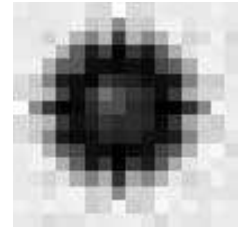


Imaginary Part

(c) Reconstructed images for FR.

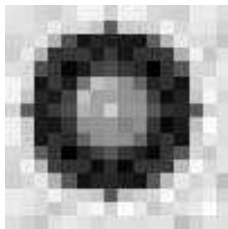


Real Part

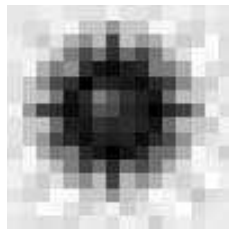


Imaginary Part

(d) Reconstructed images for Choice 2.

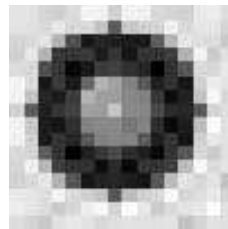


Real Part

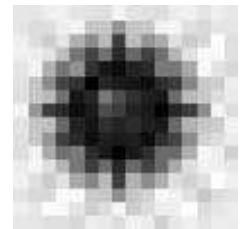


Imaginary Part

(e) Reconstructed images for HS.

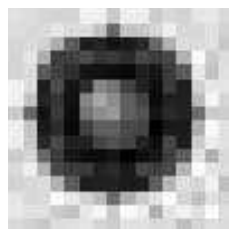


Real Part

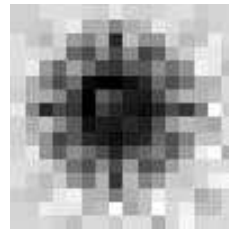


Imaginary Part

(f) Reconstructed images for Choice 3.



Real Part



Imaginary Part

(g) Reconstructed images for Choice 4.

Fig. 11. Reconstructed real and imaginary parts for test case 3 without noise using the PPR, HS, FR, Choice 1, Choice 2, Choice 3, and Choice 4 directions.

work well for reconstruction of the object, but the HS direction is slightly better. For a phase shift of about 0.75π , again all but the FR direction work well at reconstructing the real and imaginary parts of the contrast function. The YD direction is the fastest with quantitatively good reconstruction images; the reason for the speed of the YD direction is still under investigation. As the phase shift increases, the CG method begins to break down. Using an inexact line search with Wolfe conditions, it is possible to reconstruct objects with phase shifts up to 0.85π . However, reconstructing an object with a phase shift of 1.003π poses some difficulty; this is consistent with the findings in Ref. 16. Since the initial guess for the contrast function was zero, it is expected that better choice of an initial guess will significantly improve the phase shift limitation. For an object with a phase shift less than π (test cases 1 and 2) the CG method was found to be robust for an SNR of 50 dB. For objects with a phase shift much larger than π , multi-frequency techniques such as those proposed in Ref. 26 must be exploited to reduce the ill-posedness.

Our numerical experiments show that the PPR direction is not the best choice for the problem of interest. Depending on the phase shift of the object to be imaged, different methods have different merits. For an object with low contrast and a small phase shift, the HS direction works best in terms of the quality of the reconstructed images, *RRE* value, *MSE* value, and CPU time. For an object with high contrast and a large phase shift, the YD direction seems to be the best choice with respect to the CPU time. When the phase shift of the object is unknown, the YD direction is recommended. Depending on the problem and whether the emphasis is on the rate of convergence or on the CPU time, one can try different choices for the two parameters λ and μ . With the introduction of the two-parameter family of conjugate gradient directions, one has more freedom than ever before. We are aware that a large but low contrast object can have phase shifts larger than π . Due to the limitations of our computer resources, we did not investigate this problem here. It is the topic of future research.

Acknowledgments

The first author wishes to thank Dr. John L. Nazareth for his helpful suggestions, and all authors thank the reviewers for their helpful comments. This work was supported by the National Science Foundation and by the Carl M. Hansen Foundation.

References

1. W. C. Chew and Y. M. Wang, Reconstruction of two-dimensional permittivity distribution using the distorted Born iterative method, *IEEE Trans. Medical Imaging* **9** (1990) 218–225.
2. L. J. Liu, X. Zhang and S. L. Broschat, Ultrasound imaging using variations of the iterative Born technique, *IEEE Trans. Ultrasonics, Ferroelectrics, and Freq. Control* **46**(3) (1999) 574–583; *ibid.* **45**(5) (1999) 1331–1333.
3. A. Frenchois and C. Pichot, Microwave imaging—complex permittivity reconstruction with a Levenberg-Marquardt method,” *IEEE Trans. Antennas Propagat.* **45** (1997) 203–215.
4. N. Joachimowicz, C. Pichot and J.-P. Hugonin, Inverse scattering: An iterative numerical method for electromagnetic imaging, *IEEE Trans. Antennas Propagat.* **39** (1991) 1742–1752.

5. D. T. Borup, S. A. Johnson, W. W. Kim and M. J. Berggren, Nonperturbative diffraction tomography via Gaussian-Newton iteration applied to the scattering integral equation, *Ultrasonic Imaging* **14** (1992) 69–85.
6. M. R. Hestenes and E. L. Stiefel, Methods of conjugate gradients for solving linear systems, *J. Res. Nat. Bur. Stds., Section B* **49** (1952) 409–436.
7. R. Fletcher and C. Reeves, Function minimization by conjugate gradients, *Comput. J.* **7** (1964) 149–154.
8. B. T. Polyak, The conjugate gradient method in extremem problems, *USSR Comput. Math. and Math. Phys.* **9** (1969) 94–112.
9. E. Polak and G. Ribiere, Note sur la convergence de methode de directions conjuguees, *Revue Francaise d'Informatique et de Recherche Operationnelle* **16** (1969) 35–43.
10. Y. H. Dai and Y. Yuan, A nonlinear conjugate gradient method with nice global convergence properties, Research Report ICM-95-038, Institute of Computational Mathematics and Scientific/Engineering Computing, Chinese Academy of Sciences, Beijing, China, 1995.
11. J. L. Nazareth, Multialgorithms for parallel computing, Pacific Northwest Num. Analysis Seminar (PNWNAS'97), Boeing Field, Seattle, Washington, Oct. 1997.
12. H. Harada, D. J. N. Wall, T. Takenaka, and M. Tanaka, Conjugate gradient method applied to inverse scattering problem, *IEEE Trans. Antennas Propagat.* **43**(8) (1995) 784–792.
13. P. Lobel, R. Kleinman, Ch. Pichot, L. Blanc-Feraud and M. Barlaud, Conjugate gradient method for solving inverse scattering with experimental data, *IEEE Antennas Propagat. Magazine* **38**(3) (1996) 48–51.
14. R. E. Kleinman and P. M. van den Berg, Inverse scattering — a nonlinear optimization approach, ftp://poseidon.math.udel.edu/pub/Wave_Center/Reports/96.
15. R. E. Kleinman and P. M. van den Berg, A modified gradient method for two-dimensional problems in tomography, *J. Computational and Applied Mathematics* **42** (1992) 17–35.
16. T. J. Cavicchi and W. D. O'Brien, Jr., Numerical study of higher-order diffraction tomography via the sinc basis moment method, *Ultrasonic Imaging* **11** (1989) 42–74.
17. P. N. T. Wells, *Ultrasonics in Clinical Diagnosis* (Churchill Livingstone, Edinburgh, New York, 1977).
18. E. L. Madsen, H. J. Sathoff, and J. A. Zagzebske, Ultrasonic shear wave properties of soft tissues and tissue-like materials, *J. Acoust. Soc. Am.* **74** (1983) 1346–1355.
19. R. F. Harrington, *Field Computation by Moment Methods* (MacMillan, New York, 1968).
20. H. A. van der Vorst, BI-CGSTAB: A fast and smoothly converging variant of BI-CG for the solution of nonsymmetric linear systems, *SIAM J. Sc. Stat. Comput.* **13**(2) (1992) 631–644.
21. D. T. Borup and O. P. Gandhi, Calculation of high-resolution SAR distributions in biological bodies using the FFT algorithm and conjugate gradient method, *IEEE Trans. Microwave Theory and Techniques* **33**(5) (1985) 417–419.
22. J. Nocedal, Theory of algorithms for unconstrained optimizaton, *Acta Numerica* **1** (1992) 199–242.
23. P. Wolfe, Convergence conditions for ascent methods, *SIAM Review* **11** (1969) 226–235.
24. D. P. Bertsekas, *Nonlinear Programming* (Athena Scientific, Belmont, MA, 1995).
25. L. Adams and J. L. Nazareth (eds.), *Linear and Nonlinear Conjugate Gradient-Related Methods* (SIAM, Philadelphia, 1996).
26. W. W. Kim, D. T. Borup, S. A. Johnson, M. J. Berggren, and Y. Zhou, Accelerated inverse scattering algorithm for higher contrast objects, *Proc. IEEE Ultrasonics Symposium*, 1987, pp. 903–906.

Copyright of Journal of Computational Acoustics is the property of World Scientific Publishing Company and its content may not be copied or emailed to multiple sites or posted to a listserv without the copyright holder's express written permission. However, users may print, download, or email articles for individual use.